WELDING RESEARCH

SUPPLEMENT TO THE *WELDING JOURNAL*, JUNE 2002
Sponsored by the American Welding Society and the Welding Research Council

# The Stress Field Characteristics in the Surface Mount Solder Joints under Temperature Cycling: Temperature Effect and Its Evaluation

*Dynamic stress distribution was analyzed with regard to the temperature cycling history of the solder joint*

**BY Y. Y. QIAN, X. MA, AND F. YOSHIDA**

ABSTRACT. Finite element analysis is one of the few methods for obtaining stress field information on surface mount solder joints under temperature cycling because of the difficulty with the experimental method. In this study, the effect of temperature history was considered in order to avoid unilateral analysis, which takes only one time into account. Analysis results show temperature cycling leads to stress cycling and a thermal ratchetting effect, ***e.g.***, the accumulation of inelastic strain. Furthermore, stress field distribution in the solder joints had a dynamic feature during temperature cycling and was related to temperature history, such as the value and the site of maximum equivalent stress. Relative damage stress is put forward as the dominant mechanical factor because of void damage failure in solder joints and their history of dependence on stress field distribution under temperature cycling. Analysis results indicate the most dangerous condition for failure is in the high temperature hold time during temperature cycling, which correlates to already known experimental data.

## Introduction

The finite element method (FEM) has been widely used for studying the stress-strain response of solder joints under temperature cycling (Ref. 1). The applications of FEM results are 1) the inducing of cyclic inelastic strain range into the Manson-Coffin equation to predict thermal fatigue life (Refs. 2, 3); 2) predicting crack initiation sites according to the site of maximum equivalent stress or strain (Refs. 4, 5); and 3) design optimization of solder joints based on the comparison of equivalent stress distribution (Refs. 6, 7).

In application 1 above, the major focus is on the constitutive relationship of the solder alloy in order to model its nonlinear mechanical response more accurately. This study is not concerned with this. In above applications 2 and 3, the major focus is how to determine the most critical stress distribution. In the literature, conclusions were usually based on the equivalent stress distribution in the solder joint at a single time. This presents two problems: 1) the only external load is from temperature cycling, which means the stress distribution should be dynamically changing at different times during the whole temperature history. Furthermore, the mechanical properties of the solder changed with temperature. Although there is a time for the stress distribution's maximum abstract value, the solder alloy may have had its best properties at that same time. 2) Interface void damage is the main failure mechanism of the solder joint (Refs. 8–10), and such phenomenon is dependent on stress triaxiality, not equivalent stress (Refs. 11–13). Therefore, considering only equivalent stress is not suitable. In this study, we first analyzed the dynamic stress distribution in the solder joint from its temperature history. Then, a new mechanical concept was proposed in which temperature history was taken into account and used to explain the experimental data.

***Y. Y. QIAN and X. MA are with the National Key Laboratory of Welding, Harbin Institute of Technology, Harbin, P.R.C. F. YOSHIDA is with the Department of Mechanical System Engineering, Hiroshima University, Higashi-Hiroshima, Japan.***

KEY WORDS

Stress Field
Damage Stress
Solder Joint
Temperature History
Temperature Cycling

### Finite Element Modeling

A simulated surface mount assembly used for the accelerating thermal fatigue life test is shown in Fig. 1. A ceramic board (Ni-plated) was soldered with a FR-4 board (Cu pad on it) using Sn60-Pb40 solder alloy. The joining area of every solder joint was 1 x 2 mm, and the thickness of the joint was 0.2 mm. Commercial nonlinear finite element program MARC 7.0® and prepost processing program MENTAT 3.1® were used for numerical simulation and the work was carried out in a Sun-Ultral 1® workstation. Figure 2 is the corresponding two-dimen-

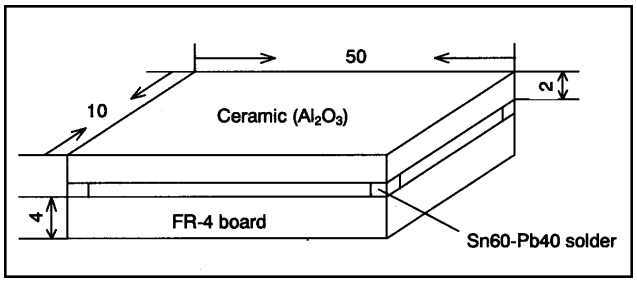


*Fig. 1 — Schematic of simulated surface mount assembly (mm).*

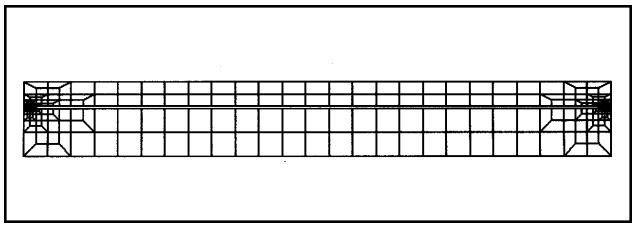

*Fig. 2 — Two-dimensional finite element model of simulated surface mount assembly shown in Fig. 1.*

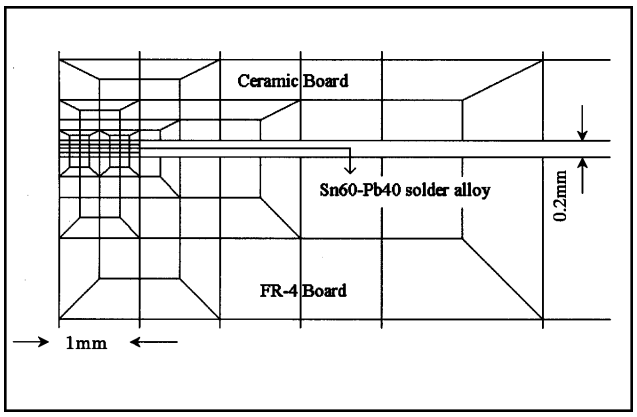


*Fig. 3 — Enlarged model of the solder joint part in Fig. 2.*

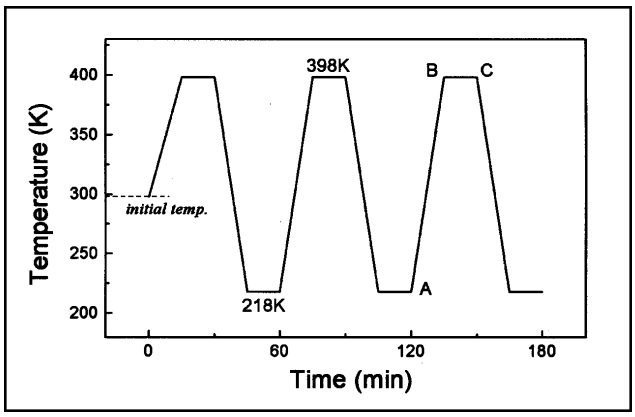


*Fig. 4 — Profile of temperature cycling load (15 min dwell time, 15 min ramp time).*

Table 1 — Material Parameters Used in FEM Calculation

| | Temperature (K) | E (MPa) | Poisson Ratio υ | CTE α ($10^{-6}$/K) | Yield Stress (MPa) |
|---|---|---|---|---|---|
| | | 131000 | 0.3 | | |
| Ceramic | 293 | | | 5.4 | |
| ($Al_2O_3$) | 316 | | | 6.6 | |
| | 349 | | | 7.4 | |
| | 411 | | | 8.5 | |
| | 473 | | | 9.2 | |
| FR-4 | | 22000 | 0.28 | 18.0 | |
| | 218 | 47966 | 0.3516 | 24.1 | 43.2 |
| Sn60Pb40 | 238 | 46892 | 0.3540 | 24.6 | 37.51 |
| Solder alloy | 258 | 45779 | 0.3565 | 25.0 | 32.05 |
| | 278 | 44377 | 0.3600 | 25.2 | 29.86 |
| | 295 | 43251 | 0.3628 | 25.4 | 29.1 |
| | 323 | 41334 | 0.3650 | 26.1 | 22.96 |
| | 348 | 39445 | 0.3700 | 26.7 | 17.4 |
| | 373 | 36854 | 0.3774 | 27.3 | 12.31 |
| | 398 | 34568 | 0.3839 | 27.9 | 9.35 |

sional finite element model and Fig. 3 is the enlarged model of the solder joint part. The mesh is made of four-node plane stress elements with a total of 364 elements and 418 nodes.

In this study, the ceramic and resin boards were assumed to be linearly elastic. The solder alloy was elastic-viscoplastic with creep and plastic deformation considered together. Its stress-strain relation is given by

$$\dot{\varepsilon}_{ij} = \dot{\varepsilon}^{el}_{ij} + \dot{\varepsilon}^{pl}_{ij} + \dot{\varepsilon}^{cr}_{ij} \quad (1)$$

where the total strain rate tensor $\dot{\varepsilon}_{ij}$ is the sum of the elastic strain rate tensor $\dot{\varepsilon}^{el}_{ij}$, the plastic strain rate tensor $\dot{\varepsilon}^{pl}_{ij}$, and the creep strain rate tensor $\dot{\varepsilon}^{cr}_{ij}$. The definition of elastic and plastic strain rate is the same as usually used in nonlinear FEM calculation. The creep strain rate is defined as (Ref. 14)

$$\dot{\varepsilon}^{cr} = B_1 D \left(\frac{\sigma_e}{E}\right)^3 + B_2 D \left(\frac{\sigma_e}{E}\right)^7 \quad (2)$$

where E is elastic module, $B_1 = 1.7 \times 10^{12}$, $B_2 = 8.9 \times 10^{24}$, D = exp(–5413/T), and $\sigma_e$ is Mises equivalent stress, which can be defined as

$$\sigma_e = \sqrt{\frac{3}{2} S_{ij} S_{ij}} \quad (3)$$

with the devitoric stress tensor

$$S_{ij} = \sigma_{ij} - \frac{1}{3}\delta_{ij}\sigma_{kk} \quad (4)$$

where $\sigma_e$ is the stress tensor and $\delta_{ij}$ is the Kronecker delta. Equation 2 was combined with the MARC program by using a user self-defined subroutine. The material properties used in FEM calculation were obtained from Ref. 15 and listed in Table 1. The load profile from temperature cycling is shown in Fig. 4.

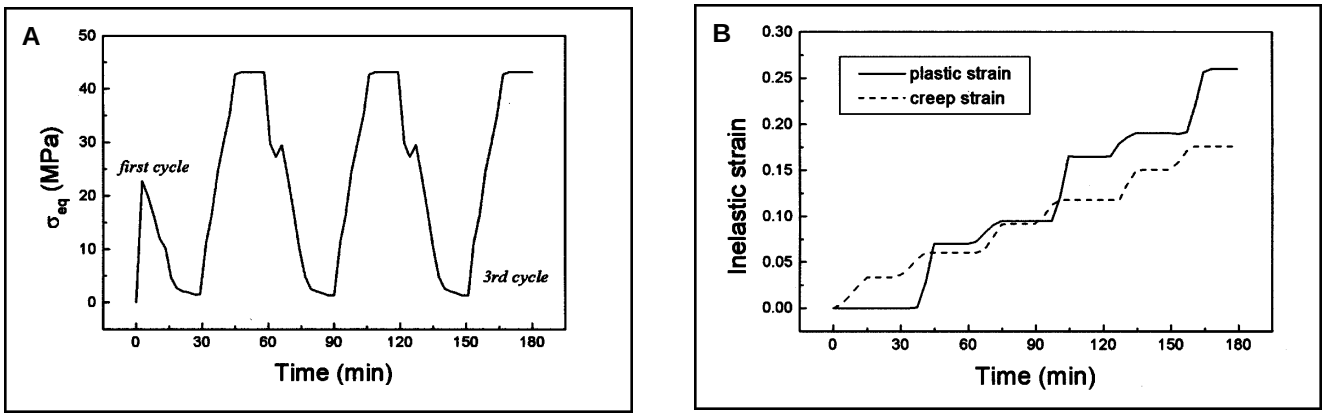


*Fig. 5 — Mechanical response history in the solder joint under temperature cycling. A — Mises equivalent stress; B — inelastic strain.*

## Simulation Results and Discussions

Since the greatest local mismatch of coefficients of thermal expansion is between the ceramic board and Sn60-Pb40 solder, the stress-strain response is obtained from the node, which is at the inner corner of the solder joint and near the ceramic/solder interface. The location is just like point A shown in Fig. 3. Figure 5 shows the equivalent stress and inelastic strain history under temperature cycling. Figure 6 is the shear stress-strain curve for five cycles. The basic feature of the stress-strain field is temperature cycling, which led to stress cycling, and this led to ratchetting behavior, ***e.g.***, the accumulation of inelastic strain. Furthermore, Fig. 5 shows the equivalent stress kept invariant during the low-temperature hold time, but relaxation occurred during high-temperature hold time. Corresponding to the times of A, B, and C during one temperature cycle in Fig. 4, the equivalent stress and shear stress distributions in the solder joint are shown in Figs. 7 and 8, which analyze the stress field under temperature cycling. The whole geometry of the stress contour shown in Figs. 7 and 8 is the same as the solder region shown in Fig. 3; therefore, its real dimension is 1 x 0.2 mm.

In Figs. 7 and 8, the stress distribution in the solder joint during the entire temperature cycle was temperature/time dependent for both the maximum stress level and the tensile or compression stress. This indicated the stress distribution in the solder joint was related to the temperature history. Although the maximum stress value occurred at the low-temperature stage, it should be noted the mechanical property of the solder alloy was also temperature dependent. Therefore, the temperature effect should be taken into account instead of the stress value alone.

### Relative Damage Stress and Failure of the Solder Joint

Failure mechanism of the solder joint is interface void damage (Refs. 8–10), and such phenomenon is dependent on stress triaxiality, not equivalent stress (Refs. 11–13). The concept of equivalent damage stress was developed by Lemaitre through thermodynamics and mesomechanics analysis in order to evaluate the damage process (Ref. 16)

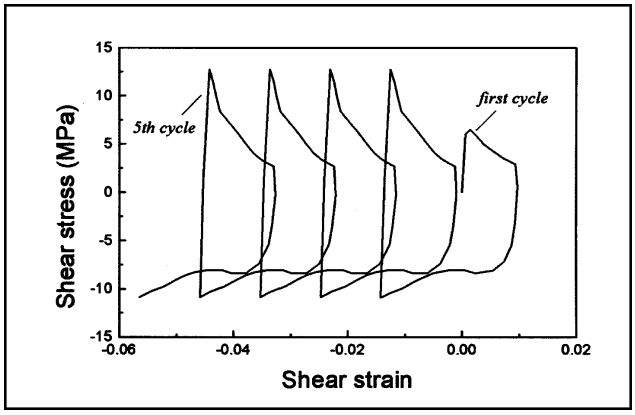


*Fig. 6 — Shear stress-strain response in the solder joint showing ratchetting behavior.*

$$\sigma^D = \sigma_{eq} R_\nu^{1/2} \quad (5)$$

where $\sigma^D$ is the equivalent damage stress, $\sigma_{eq}$ is the Mises equivalent stress, $R_\nu$ is a function of stress triaxiality as

$$R_\nu = \frac{2}{3}(1+\nu) + 3(1-2\nu)\left(\frac{\sigma_H}{|\sigma_H|}\right)\left(\frac{\sigma_H}{\sigma_{eq}}\right)^2 \quad (6)$$

where $\nu$ is the Poisson's ratio and $\sigma_H$ is the hydrostatic stress. The physics meaning of the above equation is well known: plasticity is mainly due to slips, which do not depend upon the hydrostatic stress. Cavitation damage is influenced by the hydrostatic stress or triaxiality ratio and also by Poisson's ratio, which governs the elastic volume change (Refs. 11–13, 16, 17). In order to reflect the temperature effect, Equation 5 is normalized by the material yield stress, which is the function of temperature. The new concept of relative damage stress $\sigma^*$ is defined as

$$\sigma^* = \sigma^D / \sigma_y(T) \quad (7)$$

It must be noted such a concept is a dominant mechanical factor that reflects the interface failure feature and ductile damage mechanism of the solder joint, not the failure criterion. That is to say, it is difficult to determine the occurrence of cavitation by defining a critical value of relative damage stress, but we can evaluate the possibility of cavitation initiation at a different temperature stage. Figure 9 is the relative damage stress response at the ceramic/solder alloy interface of the solder joint during the fifth temperature cycle. It was concluded that it is easiest for void damage to occur at the high-temperature hold time during temperature cycling.

Figures 10 and 11 show the experimental data for the thermal fatigue life of solder joints from Ref. 18. In Fig. 10, tem-

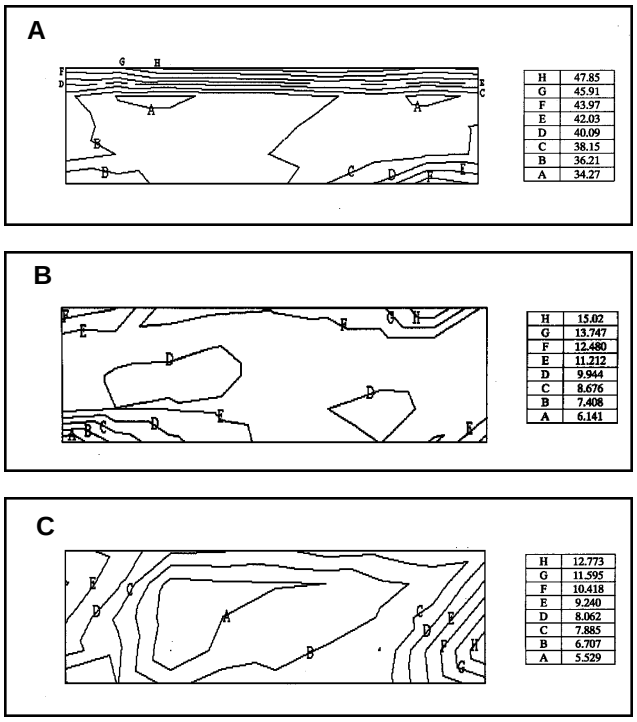


*Fig. 7 — Mises equivalent stress distribution in the solder joint at different stages during a temperature cycle (MPa): (A) at the beginning of temperature-up stage, (B) at the beginning of high-temperature hold time, and (C) at the end of high-temperature hold time.*

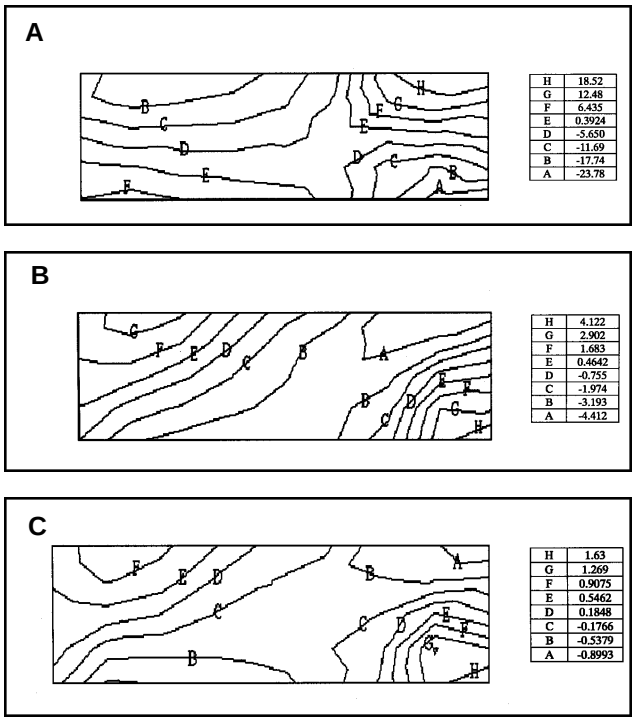


*Fig. 8 — Shear stress distribution in the solder joint at different stages during a temperature cycle (MPa): (A) at the beginning of temperature-up stage, (B) at the beginning of high-temperature hold time, and (C) at the end of high-temperature hold time.*

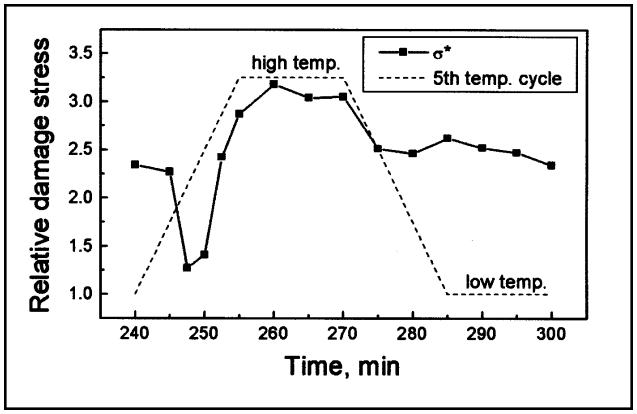


*Fig. 9 — Relative damage stress response at the ceramic/solder alloy interface of the solder joint during the fifth temperature cycle.*

perature cycling profiles A and B have the same high-temperature hold time but different low-temperature hold times. In this case, the thermal fatigue life of the solder joints was the same. In Fig. 11, profiles A and B have the same low-temperature hold time but different high-temperature hold times. In this case, the thermal fatigue life of the solder joints was different. This indicated that during temperature cycling, the high-temperature hold time has a significant effect on the reliability of the solder joints. Such phenomenon cannot be explained by a traditional mechanical concept, such as equivalent stress or strain, because their value or accumulation is very low in the high-temperature hold time (Refs. 15, 19). Some scholars had proposed dwell time was not important for the solder joint's reliability and had little meaning in the design of an accelerated thermal fatigue test (Ref. 19). But such a conclusion, based on traditional mechanical concepts, is not in agreement with the above experimental results. On the other hand, the concept of relative damage stress provides a good explanation because it has maximum value during high-temperature hold time of temperature cycling.

## Summary

Finite element numerical simulation results showed stress distribution in the solder joint was dependent on temperature cycling history. Furthermore, considering the mechanical property of the solder alloy was also temperature dependent, a new concept of "relative damage stress" was put forward. It included stress triaxiality, which promotes void damage; Mises equivalent stress, which determines plasticity; and the material yield stress, which is a function of temperature. Such a concept attempts to reflect the failure mechanism of the solder joint under temperature cycling load and is useful for evaluation of stress status in the solder joint during temperature cycling.

### *Acknowledgment*

The Association of International Education and Ministry of Education of Japan is acknowledged for its scholarship support so that X. Ma could do this work at Hiroshima University.

### *References*

1. Mackerle, J. 1997. Finite element analysis and simulation of adhesive bonding, soldering and brazing: a bibliography (1976–1996). ***Modeling Simul. Mater. Sci. Eng***. 5: 159–185.

2. Akay, H. U. 1997. Fatigue life prediction

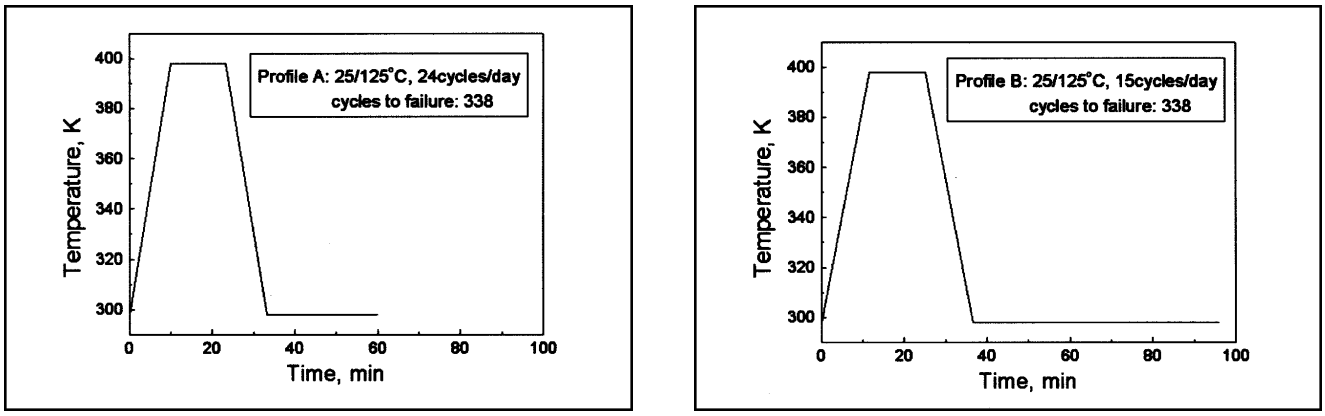


*Fig. 10 — Effect of low-temperature hold time on the thermal fatigue life of the solder joint (Ref. 18).*

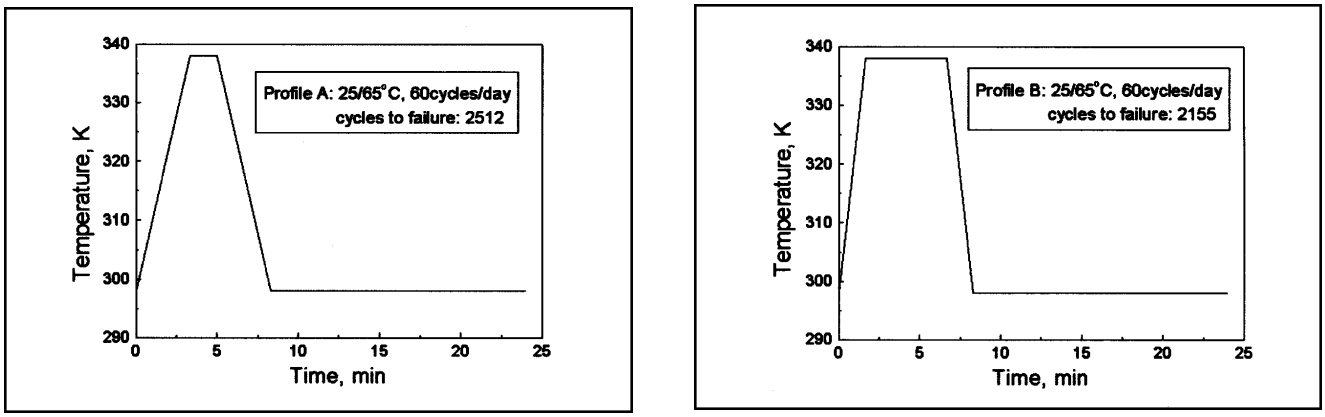


*Fig. 11 — Effect of high-temperature hold time on the thermal fatigue life of the solder joint (Ref. 18).*

for thermally loaded solder joints using a volume-weighted averaging technique. ***ASME Journal of Electronic Packaging*** 119(4): 228–235.

3. Mukai, M., Kawakami, T., Takahashi, K., Kishimoto, K., and Shibuya, T. 1998. Thermal fatigue life of solder bumps in BGA. ***JSME International Journal Series*** A 41(2): 260–266.

4. Lee, S. M., and Lee, K. W. 1996. Thermal fatigue life prediction of gull-wing solder joints in plastic thin small outline packages. ***Jpn. J. Appl. Phys.*** 35: L1515–L1517.

5. Jung, W., Lau, J. H., and Pao, Y. H. 1997. Nonlinear analysis of full-matrix and perimeter plastic ball grid array solder joints. ***ASME Journal of Electronic Packaging*** 119(3): 163–169.

6. Lau, J. H., and Harkins, C. G. 1988. Thermal-stress analysis of SOIC packages and interconnections. ***IEEE Trans. CHMT*** 11(4): 380–389.

7. Gektin, V., Bar-Cohen, A., and Ames, J. 1997. Coffin-Manson fatigue model of underfilled flip-chips. ***IEEE Trans. CPMT*** Part A 20(3): 317–325.

8. Logsdon, W. A., Liaw, P. K., and Burke, M. A. 1990. Fracture behavior of 63Sn-37Pb solder. ***Engng. Fracture Mech.*** 36: 183–218.

9. Skipor, A. F., Harren, S. V., and Botsis, J. 1995. The effect of mechanical constraint on the flow and fracture of 63/37 Sn/Pb eutectic alloy. ***Engng. Fracture Mech.*** 41: 647–669.

10. Ma, X., Qian, Y. Y., and Yoshida, F. 2000. Void damage at Sn-Pb alloy/Cu-Sn intermetallic compound interface of solder joints. ***Proc. International Brazing and Soldering Conf.*** eds. P. T. Vianco and M. Singh, pp. 568–574. American Welding Society, Albuquerque, N. Mex.

11. Varias, A. G., Suo, Z., and Shih, C. F. 1991. Ductile failure of a constrained metal foil. ***J. Mech. Phys. Solids*** 39(7): 963–986.

12. Huang, Y., Hutchinson, J. W., and Tvergaard, V. 1991. Cavitation instabilities in elastic-plastic solids. ***J. Mech. Phys. Solids*** 39(2): 223–241.

13. Huang, Y., Hu, K. X., Yeh, C. P., Li, N. -Y., and Hwang, K. C. 1996. A model study of thermal stress-induced voiding in electronic packaging. ***ASME Journal of Electronic Packaging*** 118(4): 229–234.

14. Wong, B., Helling, D. E., and Clark, R. W. 1988. A creep-rupture model for two-phase eutectic solders. ***IEEE Trans. CHMT*** 11(3): 284–290.

15. Hong, B. Z.; and Burrel, L. G. 1997. Modeling thermally induced viscoplastic deformation and low cycle fatigue of CBGA solder joints in a surface mount package. ***IEEE Trans. CPMT*** Part A 20(3): 280–285

16. Lemaitre, J. 1996. ***A Course on Damage Mechanics.*** p. 45. New York, N.Y: Spring-Verleg.

17. Ashby, M. F., Blunt, F. J., and Bannister, M. 1989. Flow characteristics of highly constrained metal wires. ***Acta Metall.*** 37(7): 1847–1857.

18. Pan, T. Y. 1994. Critical accumulated strain energy (case) failure criterion for thermal cycling fatigue of solder joints. ***ASME Journal of Electronic Packaging*** 116(3): 163–170.

19. Yu, Q., and Shiratori, M. 1997. Fatigue-strength prediction of microelectronics solder joints under thermal cyclic loading. ***IEEE Trans. CPMT*** Part A 20(3): 266–273.